Andean subduction-related mantle xenoliths: Isotopic evidence of Sr–Nd decoupling during metasomatism

R.V. Conceição[a,b,*], G. Mallmann[b,c], E. Koester[b], M. Schilling[d], G.W. Bertotto[e], A. Rodriguez-Vargas[f]

[a]*Departamento de Geologia, Universidade Federal do Rio Grande do Sul, Av. Bento Gonçalves 9500, C.P. 15001, 91501-970, Porto Alegre, RS, Brazil*
[b]*Laboratório de Geologia Isotópica, CPGq, Universidade Federal do Rio Grande do Sul, CEP 91501970, Porto Alegre, Brazil*
[c]*Programa de Pós-graduação em Geociências, CNPq, Universidade Federal do Rio Grande do Sul, CEP 91501970, Porto Alegre, Brazil*
[d]*Facultad de Ciencias Fisicas y Matematicas, Universidad de Chile, Santiago 4058, Chile*
[e]*CONICET, Facultad de Ciencias Exactas y Naturales, Universidade Nacional de La Pampa, Santa Rosa 644, Argentina*
[f]*Universidad Nacional de Colômbia, 4452 Bogotá, Colombia*

Abstract

Sr–Nd isotopic analyses on some mantle xenolith samples from the Northern, Southern and Austral Andean volcanic zones exhibit radiogenic Sr enrichment without dramatic changing of the Nd isotopic composition. This anomalous effect (Sr–Nd decoupling) makes these samples plot displaced to the right side of the "mantle array" trend (here called the "MORB–OIB–BSE trend") in the $^{87}Sr/^{86}Sr$ vs. $^{143}Nd/^{144}Nd$ isotopic diagram. Such behavior reflects processes that took place in the mantle and can be related to: i) the mixture of a depleted mantle and an enriched source (enriched mantle II—EMII); ii) the mixture of a depleted mantle and a mixture of mantle-derived and slab-derived melts; and iii) a chromatographic process that occurs during the percolation of a metasomatic agent through the mantle.

Keywords: Mantle; Xenoliths; Metasomatism; Andes; Sr–Nd isotopes, Chromatography

1. Introduction

The lithospheric mantle, assumed as the portion of the lithosphere below the Mohorovicic discontinuity and above the asthenosphere, can be defined in terms of its chemical, thermal, seismic and/or mechanical properties. Simple petrological and chemical models have been proposed for the bulk composition and

* Corresponding author. Departamento de Geologia, Universidade Federal do Rio Grande do Sul, Av. Bento Gonçalves 9500, C.P. 15001, 91501-970, Porto Alegre, RS, Brazil. Tel.: +55 51 3316 7140; fax: +55 51 3316 7270.
E-mail address: rommulo.conceicao@ufrgs.br (R.V. Conceição).

mineralogy of the oceanic lithospheric mantle (e.g. Ringwood, 1982; Menzies and Hawkesworth, 1987). However difficulties have arisen for a precise understanding of the subcontinental lithospheric mantle composition and mineralogy due to its long-term evolution and the occurrence of processes responsible for its continuous compositional changes (McDonough and Frey, 1989; McDonough, 1990; Mukasa and Wilshire, 1997).

Besides melting and convection, another important process that occurs in the mantle is metasomatism, which is defined as the percolation of fluids or melts through the solid mantle, inducing chemical and, in some cases, modal changes (see Menzies and Hawkesworth, 1987 and references therein). The metasomatic agent has been attributed to products derived either from the asthenosphere underneath the subcontinental lithosphere, or from the subducted slab in compressive regimes. In both cases, and in a simple constrain, the isotopic composition of the subcontinental lithospheric mantle, initially characterized by impoverishment of radiogenic Sr (decreasing of the $^{86}Sr/^{87}Sr$ ratio), enrichment of radiogenic Nd (increasing of the $^{143}Nd/^{144}Nd$ ratio) and depletion of incompatible elements due to melting, must change during metasomatism due to incorporation of more radiogenic Sr, less radiogenic Nd and enrichment of incompatible elements.

The composition of the metasomatic agent has been discussed in several papers (see Menzies and Hawkesworth, 1987 and references therein), but emphasis has been put on carbonatite-rich melts (e.g. Yaxley et al., 1991, 1998), K-enriched silicic melt (e.g. Conceição and Green, 2000, 2004) and/or highly alkaline (Na_2O+K_2O+CaO) silicic melt (Hirschman et al., 1998a,b) due to their unusual compositions, and possibility of being direct partial melts from the mantle or from a subducted lithosphere. A simplistic model of interaction between these metasomatic agents and the mantle assumes that the metasomatic agent will be mixed with the depleted mantle lithosphere by a "two-end-member simple mixture process" (Faure, 1986). Such a process does not consider reactions that could take place due to the diversity of the depleted mantle mineralogy, which accounts for different partition coefficients for Sm, Rb, Nd and Sr. Some authors, however, call attention to this possibility and refer to it as a chromatographic process (Hoffmann, 1988; Navon and Stolper, 1987; Godard et al., 1995; Bedini et al., 1997; Hauri, 1997).

This paper presents new results of Rb–Sr and Sm–Nd systematic isotopic analyses carried out on five ultrabasic mantle xenoliths suites sampled from Northern, Southern and Austral volcanic zones of the Andean Cordillera. Also, we briefly present and discuss new data on trace and rare earth element analyses.

2. South American mantle xenoliths and the analyzed samples

The western South American plate is a natural laboratory for petrological investigations of the subcontinental lithosphere due to the complex tectonic configuration of the Andes. This complexity is established by the configuration of an active continental margin in which two oceanic plates (Nazca and Antarctic) with different velocities subduct under a continental margin formed by several accretion events. Together with this, variations of the subduction angles along the active margin and the presence of seismic and asseismic ridges point towards four distinctive zones of active volcanism (Ramos, 1999): the Northern, Central, Southern and Austral volcanic zones (NVZ, CVZ, SVZ and AVZ, respectively, Fig. 1). Flat-slab segments without evidence of volcanism separate these zones, except the SVZ and AVZ that are separated by the subduction of the Chile Seismic Ridge. This last ridge encompasses the limit between the Nazca and Antarctic plates. Spinel- and/or garnet-bearing ultrabasic mantle xenoliths, associated with alkaline basalts, have been frequently described from all zones, except in the CVZ, where crust appears to be thicker than in the other zones.

This study attempts a synthesis of the observations on 22 ultrabasic mantle xenoliths that came from five separate alkaline basalt centers in the Cenozoic to Recent volcanoes from South America (Fig. 1). From north to south, these centers are: Mercaderes (NVZ—Colombia—01°45′N, 77°03′W), Agua Poca (SVZ—Argentina—37°01′S, 67°07′W), Cerro del Mojon (SVZ—Argentina—41°06′S, 70°13′W), Lote 17 (AVZ—Argentina—48°30′S, 70°30′W) and Cerro Redondo (AVZ—Argentina—49°07′S, 70°08′W). Petrographic and geochemical characterization of all these xenoliths was described in Weber (1998),

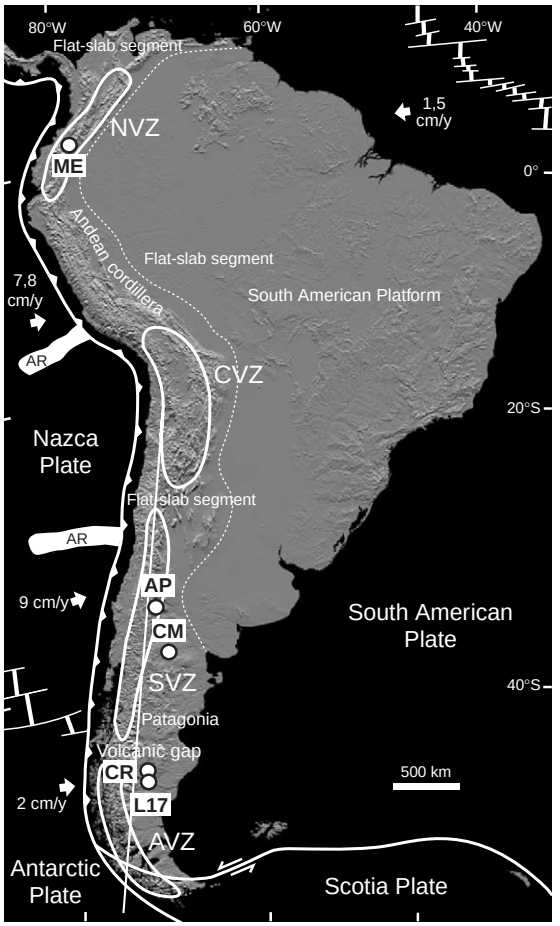

Fig. 1. Plate tectonics setting of the South American continent showing the Andean active volcanic zones (Northern—NVZ, Central—CVZ, Southern—SVZ, Austral—AVZ) and asseismic ridges (AR). Circles indicate studied samples localities: ME—Mercaderes, AP—Agua Poca, CM—Cerro del Mojon, L17—Lote 17, CR—Cerro Redondo. Modified after Ramos (1999).

Bertotto (2000), Conceição et al. (2003), Schilling et al. (2005) and Rodriguez-Vargas et al. (2005). A summary of petrographic and geochemical characteristics and the *P–T* estimates for the last equilibration of these xenoliths in the upper mantle are given in Tables 1 and 2.

3. Analytical techniques

Major element for each sample was determined by X-ray fluorescence (XRF), with loss on ignition (LOI) determined gravimetrically at the Universidade Federal do Rio Grande do Sul, Brazil. For trace and rare earth elements and isotopic analyses, around 0.5 to 0.8 g of each sample was crushed in an agate mortar and leached with HCl 0.1 N in order to eliminate the crustal alteration. Then, the leached residue was digested with HF, HNO_3, HCl and a solution was prepared in HCl 2.5 N. For trace and rare earth elements, part of this solution was diluted by a factor of 4000 and a Re/In external standard was added to the solution. Trace and rare earth element concentrations were determined on Inductively Coupled Plasma-Mass Spectrometer (ICP-MS, Elan 6000, Perkin Elmer), in which light and heavy elements were corrected based on In and Re concentrations, respectively. For isotopic analyses, an aliquot of the HCl 2.5 N solution was spiked with mixed ^{87}Rb–^{84}Sr and ^{149}Sm–^{150}Nd tracers in Teflon vials and warmed for one week on a hot plate until complete mixing. Column procedures used cationic AG-50W-X8 (200–400 mesh) resin in order to separate Rb, Sr and REE, followed by Sm and Nd separation using anionic LN-B50-A (100–200 μm) resin. Each sample was dried to a solid and then loaded with 0.25 N H_3PO_4 (Rb, Sr, Sm and Nd), on appropriate filaments (single Ta for Rb, Sr, Sm, and triple Ta–Re–Ta for Nd). The samples were run in a multi-collector VG Sector 54 thermal ionisation mass spectrometer at the Laboratório de Geologia Isotópica (Universidade Federal do Rio Grande do Sul, Brazil) in static mode. Sr and Nd ratios were normalized to $^{86}Sr/^{88}Sr=0.1194$ and $^{146}Nd/^{144}Nd=0.7219$, respectively. Measurements for the NIST standard NBS-987 gave $^{87}Sr/^{86}Sr=0.710260\pm0.000014$, La Jolla gave $^{143}Nd/^{144}Nd=0.511859\pm0.000010$. Blanks were <60 pg for Sr, <500 pg for Rb, <150 pg for Sm and <500 pg for Nd.

4. Major and trace element compositions

New whole-rock major and trace element analyses of studied mantle xenoliths, besides those presented in Bertotto (2000), Schilling et al. (2005) and Rodriguez-Vargas et al. (2005) are listed in Tables 1 and 2. Based on the Ca/Al and Na/Al ratios (McDonough, 1990), sample AND-01 from Lote 17 is the most fertile compared to the other samples (Fig. 2). Samples 4-F3,

Table 1
Modal compositions, petrographic textures, some major element compositions, Mg# [(MgO/(MgO+FeO))*100], and pressure (*P*) and temperature (*T*) conditions of the studied samples

	Northern volcanic zone								Southern volcanic zone							Austral volcanic zone						
	Mercaderes								Agua Poca			Cerro del Mojon				Lote 17	Cerro Redondo					
	XM-3	XM-5	XM-4	XM-1	XM-2	XM-6	XM-7	XM-8	AP-75	AP-80	AP-91b	4-B8	4-B9	4-C2	4-F3	AND-01	X-B	X-C	X-D	X-E	X-F	X-G
Modal composition (%)																						
Ol			2.7		0.3				58.1	71.3	64.3	70.2	84.7	57.9	1.1	69.2	70.1	62.0	71.6	72.8	57.1	60.6
Cpx	67.3	65.4	9.2	2.8	3.6	31.9	42.3	72.8	20.0	10.4	13.9	3.6	3.1	13.5	92.8	17.4	8.4	11.3	11.4	11.8	3.0	10.9
Opx	18.4	27.1	6.3	86.5	1.3	10.6	32.2	11.4	18.2	15.6	18.7	23.5	10.6	9.4	0.5	12.3	19.7	23.8	15.7	12.6	38.4	27.8
Sp	8.2	7.5		5.5		0.2	3.5	2.5	3.7	2.7	3.1	2.7	1.7	0.7	5.5	1.1	1.8	2.9	1.3	2.9	1.5	0.7
Grt			22.3	4.4	59.5	54.0	19.0	10.5														
Amph	6.0		0.6	0.7		2.8	3.0	2.8						0.4								
Melt														18.1								
Groundmass					35.0																	
Classification, texture and geochemistry (wt.%)																						
Rock/Min.	Webst	Webst	Lherz	Webst	Lherz	Webst	Webst	Webst	Lherz	Lherz	Lherz	Harzb	Harzb	Lherz	Cpxite	Lherz	Lherz	Lherz	Lherz	Lherz	Harzb	Lherz
Texture	Proto	Proto	Porph	Proto	Porph	Proto	Proto	Proto	Porph	Porph	Porph	Pro–Por	Pro–Por	Porph	Proto	Proto	Proto	Proto	Proto	Proto	Proto	Proto
Special features			React. rims, serp. veins	React. rims	React. rims, serp.		React. rims	React. rims				React. Cpx-Sp		Melt pockets	Basalt react.		Veined, basalt react.	Veined	Veined	Veined	Veined	Veined
Mg#		87.35	89.83	91.43		83.86	80.97		88.98	91.87	89.87	91.34	91.07	90.63	63.57	90.20	88.87	90.15	90.71	90.38	91.11	91.03
CaO		20.00	2.08	1.55		9.51	6.77		4.06	2.10	3.17	0.71	0.69	1.71	17.55	2.11	2.16	1.78	1.16	1.44	0.97	1.28
Na_2O		0.42	2.45	0.03		0.61	0.15		0.3	0.17	0.18	0.22	0.23	0.36	1.50	0.29	0.71	0.35	0.18	0.26	0.20	0.23
Al_2O_3		4.26	0.08	3.47		16.74	12.73		3.81	2.79	3.57	1.33	1.04	1.90	11.17	1.72	3.47	2.26	2.07	1.69	1.94	1.90
Equilibration T and P																						
T (°C)	1065		1140–1175	1250–1295					960–1099			936–993				970–1005	830–1095					
P (GPa)	1.6		>3.8	3.5					1.0–1.8			1.5–2.0				0.8–2.5	1.2–2.1					

Data are from this study and from: (i) Rodriguez-Vargas et al. (2005) and Weber (1998) (Mercaderes); (ii) Bertotto (2003) (Agua Poca); Schilling et al. (2005) (Cerro Redondo). Min.=mineral, Ol=olivine, Cpx=clinopyroxene, Opx=orthopyroxene, Sp=spinel, Grt=garnet, Amph=amphibole, Webst=websterite, Lherz=lherzolite, Harz=harzburgite, Cpxite=clinopyroxenite. Proto=protogranular, Porph=porphyroclastic, Pro–Por=protogranular to porphyroclastic, React.=reaction, Serp.=serpentine. Textures described according to Mercier and Nicolas (1975). Pressure and temperature were estimated based on the following works: Brey and Köhler (1990), for *P*, and Köhler and Brey (1990), for *T*, were used for Mercaderes, Agua Poca, Cerro del Mojon and AND-01 samples. Mercier et al. (1984), for *P* and Wood and Banno (1973), for *T*, were used for Cerro Redondo samples. Pressure and temperature for the other samples from Gobernador Gregores (Lote 17) studied by Gorring and Kay (2000) were obtained from their work.

Table 2
Geochemical and isotopic data of the studied samples

	Northern volcanic zone								Southern volcanic zone							Austral volcanic zone						
	Mercaderes								Agua Poca			Cerro del Mojon				Lote 17		Cerro Redondo				
	XM-3	XM-5	XM-4	XM-1	XM-2	XM-6	XM-7	XM-8	AP-75	AP-80	AP-91b	4-B8	4-B9	4-C2	4-F3	AND-01	Cpx	X-B	X-C	X-D	X-E	X-F	X-G
Trace elements (ppm), except for K_2O and P_2O_5 (wt.%)																							
Ba	6.18	86.26	14.35	8.22	6.10	31.39	63.29	23.90	nd	2.00	4.00	1.29	2.31	13.13	79.56	2.73		88.00	36.00	41.00	15.00	13.00	12.00
Rb	0.14	0.92	0.25	0.21	0.06	0.62	0.16	0.42	0.20	0.03	0.04	2.12	0.49	1.37	3.90	0.07		6.73	2.72	0.71	0.25	0.92	0.19
Th	nd	nd	nd	nd	nd	nd	nd	nd	nd	0.09	nd	0.07	0.03	0.05	0.37	0.04		2.00	2.00	2.00	1.00	1.00	1.00
K_2O	nd	0.01	0.01	0.01	nd	0.02	0.01	nd	0.03	nd	0.02	0.04	0.02	0.10	0.24	0.01		0.36	0.06	0.01	0.05	0.04	0.03
Nb	nd	4.00	3.00	4.00	nd	4.00	4.00	nd	1.00	nd	nd	0.14	0.16	0.79	3.41	0.08		6.00	2.00	2.00	2.00	2.00	2.00
Ta	nd	nd	nd	nd	nd	nd	nd	nd	nd	nd	nd	0.19	0.13	0.34	0.34	0.12							
La	0.26	0.38	0.12	0.10	0.48	0.44	0.68	2.75	nd	0.06	0.18	0.38	0.29	0.68	5.20	0.23		5.00	1.70	0.35	0.65	0.26	0.25
Ce	1.15	0.96	0.33	0.24	1.47	1.31	2.20	11.32	nd	0.24	0.81	0.84	0.64	2.14	17.57	0.71		13.10	3.90	0.90	1.40	0.60	0.60
Sr	96.08	25.80	6.75	6.91	26.38	23.63	19.86	81.37	9.55	3.00	8.00	5.48	7.69	38.85	216.31	7.94		127.77	42.56	6.93	5.05	15.67	5.01
Nd	1.39	2.53	0.12	0.80	1.53	0.89	1.82	3.18	nd	0.23	0.92	0.43	0.37	1.75	18.59	0.67		6.95	2.40	0.55	0.85	0.45	0.46
P_2O_5	nd	0.01	0.01	0.01	nd	0.02	0.16	nd	0.04	nd	0.02	0.01	0.01	0.02	0.06	0.01		0.13	0.05	0.03	0.05	0.04	0.03
Sm	0.36	1.04	0.05	0.20	0.66	0.39	0.78	3.29	nd	0.11	0.37	0.09	0.09	0.47	5.38	0.20		1.28	0.33	0.13	0.21	0.12	0.15
Zr	nd	10.00	13.00	9.00	nd	22.00	24.00	nd	5.17	12.00	15.00	2.80	1.83	5.12	73.33	3.88		46.00	18.00	6.00	6.50	3.50	3.70
Hf	nd	nd	0.53	nd	0.21	0.36	0.47	1.71	nd	0.10	0.20	0.07	0.04	0.17	2.74	0.13		2.40	1.60	1.60	2.60	3.30	3.20
Ti	nd	1220	990	490	nd	2260	1830	nd	1600	910	1350	110	168	625	7899	817		3500	1300	500	900	600	900
Y	nd	5.61	2.24	nd	29.45	17.66	34.86	11.15	4.88	2.70	4.00	0.49	0.43	1.82	20.10	0.99		3.70	1.90	1.10	1.30	1.10	1.20
Yb	nd	0.64	0.27	0.10	4.46	3.29	5.32	0.77	nd	0.32	0.46	0.06	0.05	0.17	1.79	0.11		0.21	0.17	0.12	0.16	0.15	0.15
Rare earth elements (ppm)																							
La	0.26	0.38	0.12	0.10	0.48	0.44	0.68	2.75		0.06	0.18	0.38	0.29	0.68	5.20	0.23		5.00	1.70	0.35	0.65	0.26	0.25
Ce	1.15	0.96	0.33	0.24	1.47	1.31	2.20	11.32		0.24	0.81	0.84	0.64	2.14	17.57	0.71		13.10	3.90	0.90	1.40	0.60	0.60
Pr	0.19	0.19	0.79	nd	0.35	0.20	0.36	2.23		0.05	0.15	0.11	0.08	0.34	3.39	0.13							
Nd	1.06	1.21	0.36	0.14	2.23	1.31	2.39	12.94		0.41	0.92	0.43	0.37	1.75	18.59	0.67		6.95	2.40	0.55	0.85	0.45	0.46
Sm	0.29	0.47	0.16	nd	0.87	0.54	0.99	4.05		0.18	0.37	0.09	0.09	0.47	5.38	0.20		1.28	0.33	0.13	0.21	0.12	0.15
Eu	0.10	0.19	0.07	nd	0.37	0.25	0.40	1.16		0.08	0.14	0.03	0.02	0.15	1.67	0.07		0.36	0.15	0.06	0.08	0.04	0.06
Gd	0.26	0.67	0.35	nd	1.65	0.99	2.01	3.75		0.29	0.53	0.09	0.08	0.45	5.34	0.22		1.00	0.43	0.15	0.26	0.15	0.20
Tb	nd	0.14	nd	nd	0.44	0.28	0.54	0.56		0.06	0.10	0.02	0.01	0.06	0.78	0.03							
Dy	0.19	0.96	0.36	nd	3.88	2.32	4.51	2.62		0.42	0.67	0.09	0.08	0.38	4.54	0.20		0.78	0.39	0.19	0.26	0.20	0.24
Ho	nd	0.21	nd	nd	1.02	0.63	1.18	0.41		0.10	0.15	0.02	0.02	0.07	0.86	0.04		0.13	0.07	0.04	0.05	0.05	0.05
Er	nd	0.66	0.27	nd	3.93	2.48	4.59	1.03		0.30	0.44	0.05	0.05	0.20	2.26	0.12		0.21	0.18	0.12	0.15	0.14	0.15
Tm	nd	0.10	nd	nd	0.66	0.45	0.78	0.13		0.05	0.07	0.01	0.01	0.03	0.30	0.02							
Yb	nd	0.64	0.27	0.10	4.46	3.29	5.32	0.77		0.32	0.46	0.06	0.05	0.17	1.79	0.11		0.21	0.17	0.12	0.16	0.15	0.15
Lu	nd	0.09	0.05	nd	0.71	0.56	0.86	0.11		0.05	0.07	0.01	0.01	0.03	0.25	0.02		0.03	0.02	0.07	0.02	0.02	0.03
Isotopic data																							
Sr (ppm)	96.10	25.80	6.70	6.90	26.40	23.60	19.90	81.40	8.15	2.59	8.38	2.47	3.33	22.28	145.55	4.56	61.01	127.77	42.56	6.93	5.01	5.05	15.67
Rb (ppm)	0.10	0.90	0.30	0.20	0.10	0.60	0.20	0.40	0.20	0.01	0.01	1.39	0.23	0.82	0.06	<0.01	<0.01	6.73	2.72	0.71	0.19	0.25	0.92
$^{87}Rb/^{86}Sr$	0.00422	0.10373	0.10973	0.08968	0.00648	0.07660	0.02354	0.01508	0.07132		0.00147	1.64204	0.20287	0.10662	0.00121			0.15338	0.18615	0.29921	0.10987	0.14325	0.17090
$^{87}Sr/^{86}Sr$	0.70300	0.70534	0.70410	0.70410	0.70438	0.70423	0.70432	0.70446	0.70394	0.70446	0.70426	0.71260	0.70505	0.70377	0.70269	0.70650	0.70684	0.70442	0.70467	0.70504	0.70501	0.70519	0.70479
Nd (ppm)	1.40	2.50	0.10	0.80	1.50	0.90	1.80	3.20		0.23		0.11	0.10	0.57	11.96	0.24	5.02	5.33	0.35	1.69	0.23	0.24	0.63
Sm (ppm)	0.40	1.00	0.01	0.20	0.70	0.40	0.80	3.30		0.11		0.02	0.02	0.15	3.37	0.07	1.43	1.08	0.37	0.10	0.08	0.08	0.17
$^{147}Sm/^{144}Nd$	0.15728	0.24955	0.24037	0.15595	0.26012	0.26939	0.26072	0.62596		0.30212		0.11777	0.14424	0.15538	0.17058	0.17308	0.17258	0.12289	0.64304	0.03616	0.21659	0.19472	0.15832
$^{143}Nd/^{144}Nd$	0.51308	0.51293	0.51349	0.51316	0.51288	0.51287	0.51295	0.51276		0.51342		0.51258	0.51273	0.51298	0.51273	0.51267	0.51263	0.51279	0.51291	0.51282	0.51276	0.51297	0.51284

Data are from this study are from: (i) Rodriguez-Vargas et al. (2005) and Weber (1998) (Mercaderes); (ii) Bertotto (2000) (Agua Poca); Schilling et al. (2005) (Cerro Redondo). n.d.=not detected. <0.01=lower than detection limit.

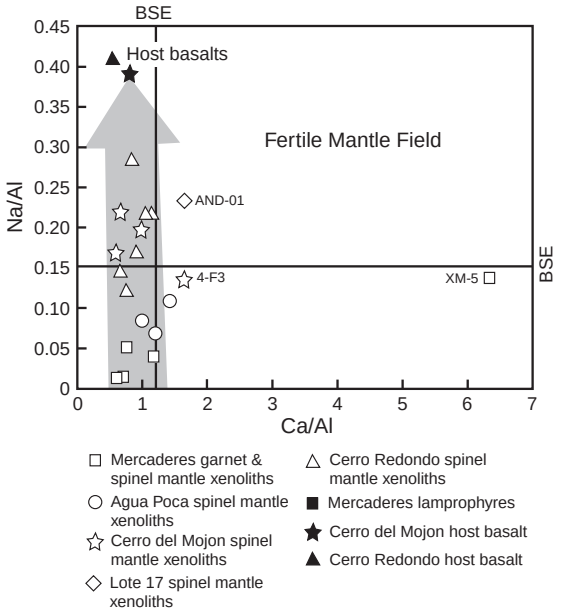

Fig. 2. Disposal of the studied samples in the Ca/Al vs. Na/Al diagram, following McDonough (1990). BSE=Bulk Earth Silicate (Zindler and Hart, 1986). See text for details. Arrow shows the trend of increasing Na/Al ratio from Mercaderes to Cerro Redondo xenoliths in the direction of the host basalts.

from Cerro del Mojon center, and XM-5, from Mercaderes center, which present the highest Ca/Al ratios, tend to follow this behavior. A trend of increasing Na/Al ratio is observed from Mercaderes to Cerro Redondo xenoliths in the direction of the host basalts. Such trend may give clues about host basalt contamination, which will be discussed in detail later on this work.

Rare earth element (REE) and trace elements of the studied xenoliths are listed in Table 2 and represented in Figs. 3 and 4. Mercaderes samples (Fig. 3A) present three REE patterns that are distinguished from the others by: (i) a strong LREE-depleted ($(La/Sm)_N$=0.36 to 0.52) and HREE enriched ($(Gd/Lu)_N$=0.24 to 0.31 and HREE around 10× chondrite) pattern; (ii) a smooth LREE-depleted ($(La/Sm)_N$=0.48 to 0.53) and almost flat to enriched MREE and HREE ($(Gd/Lu)_N$=0.84 to 1.02 and HREE around 2× chondrite) pattern; and (iii) a LREE enriched ($(La/Sm)_N$=0.44 to 0.65) and HREE depleted ($(Gd/Lu)_N$=3.94) pattern, including samples with HREE contents below the analytical detection limit. Such diversity of REE patterns reflects the complexity of the mantle evolution underneath this region. Patterns with enriched HREE are generally related to mantle that has undergone several partial-melting processes, while LREE enrichment suggests metasomatic process. The trace element patterns for these xenoliths (Fig. 4A) are strongly variable among samples. Rb

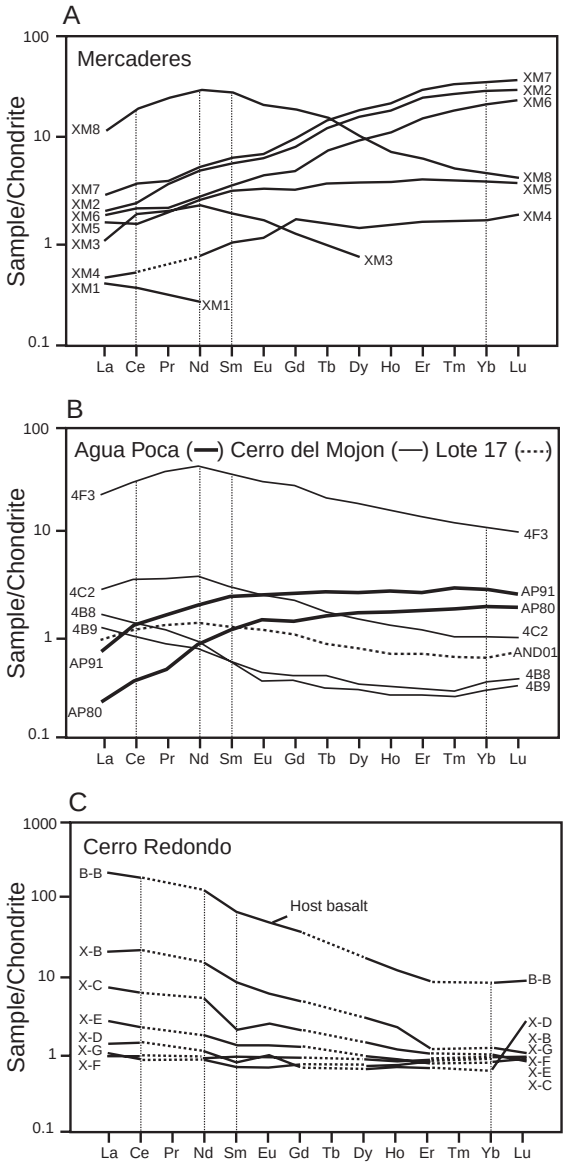

Fig. 3. REE diagram of the studied samples (A—Mercaderes, B—Agua Poca, Cerro del Mojon, Lote 17, C—Cerro Redondo) normalized for the chondrite of Sun and McDonough (1989). See text for details.

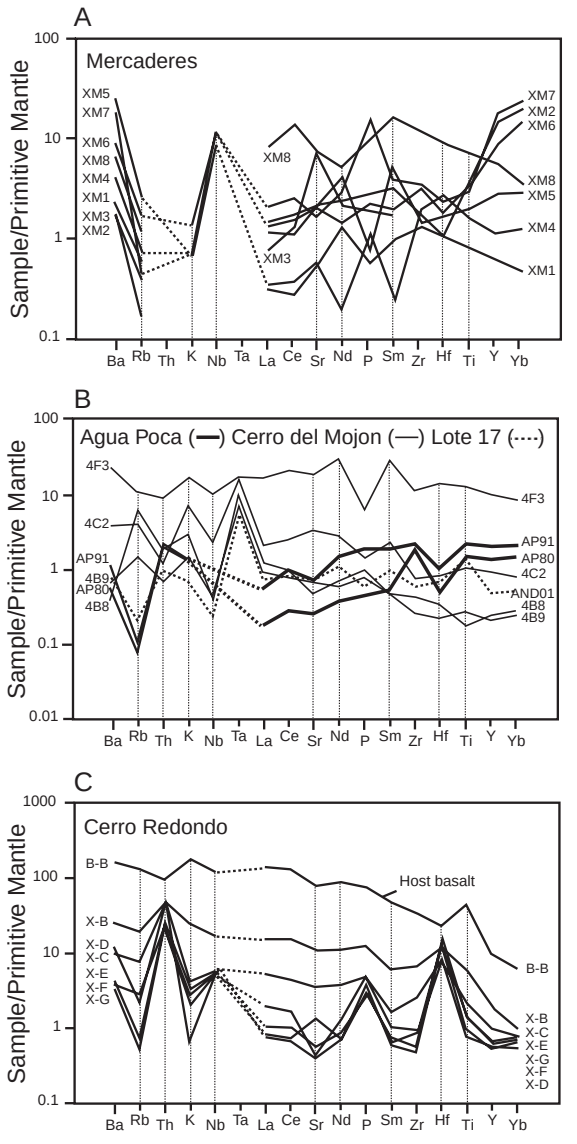

Fig. 4. Trace element spidergrams of the studied samples (A—Mercaderes, B—Agua Poca, Cerro del Mojon, Lote 17, C—Cerro Redondo) normalized for primitive mantle composition of Thompson (1982). See text for details.

and K yield strong negative anomalies, while Nb shows positive anomalies in all samples. Ba shows concentrations from around 10× to 100× chondrite, but in all cases, it shows a positive anomaly relative to Rb. This feature suggests that metasomatic processes took place in some of these samples, such those enriched in LREE. Any attempt to correlate the presence of garnet or spinel, as well as amphibole with trace element concentration is not straightforward. However, the XM-3 sample, which has the highest amphibole modal composition, is also the most Sr enriched, and has enrichment in LREE, compatible with metasomatic process.

Samples from Agua Poca (Fig. 3B) are distinguished by LREE-depleted $((La/Sm)_N$=0.22 to 0.32) and almost flat and enriched MREE and HREE patterns ($(Gd/Lu)_N$=0.73 to 0.93 and HREE around 2× chondrite), resembling Mercaderes REE patterns. They are characterized by strong Rb and Hf negative anomalies (Fig. 4B), slight Sr negative anomaly and variable positive anomalies in Th, Ce and Zr. Such characteristics are typical of a mantle that has undergone several melting processes (McKenzie, 1984; Ionov et al., 2002).

Samples from Cerro del Mojon (Fig. 3B) present two patterns, both HREE fractionated in relation to LREE. However, one of this group exhibits LREE enrichment (up to 3× chondrite in the 4-C2 sample and 34× chondrite in the 4-F3 sample), with a convex upward LREE pattern and smooth decreasing HREE contents, while the other group is better characterized by low LREE enrichment (0.89 to 1.16× chondrite) and a "U"-shaped REE pattern. Convex upward chondrite normalized REE pattern is characteristic of modally metasomatized mantle (Reiners, 1998; Ionov et al., 2002), which is consistent with the presence of amphibole and melt pockets in the sample 4-C2. The second group is characteristic of cryptic metasomatism (Menzies and Hawkesworth, 1987 and references therein). Rb, K and Ta positive anomalies, and Th and Nb negative anomalies (Fig. 4B) are also characteristic of these xenoliths, except for the sample 4-F3, which shows petrographic evidence of host basalt contamination such as clinopyroxene reaction rims, and basaltic veins.

Lote 17 (AND-01) sample is well characterized by a symmetrically shaped REE pattern around chondritic values (Fig. 3B) with concave upward LREE (summit on Nd=1.43× chondrite) and convex downward HREE patterns (summit on Tm=0.65× chondrite). High field strength elements and large ion lithophile elements variation diagrams (Fig. 4B) are similar to those for the primitive mantle, except by: a) a very positive anomaly of Ta, which gives very low Nb/Ta ratios (0.67), when compared to chondritic and

primitive mantle ratios (McDonough, 1990); b) a slightly positive Ti anomaly that gives a subchondritic and sub-primitive mantle Ti/Eu ratio of 670; and c) a negative anomaly of Rb, Nb and P. These patterns and anomalies suggest that the region from where this xenolith derived has undergone some partial melting

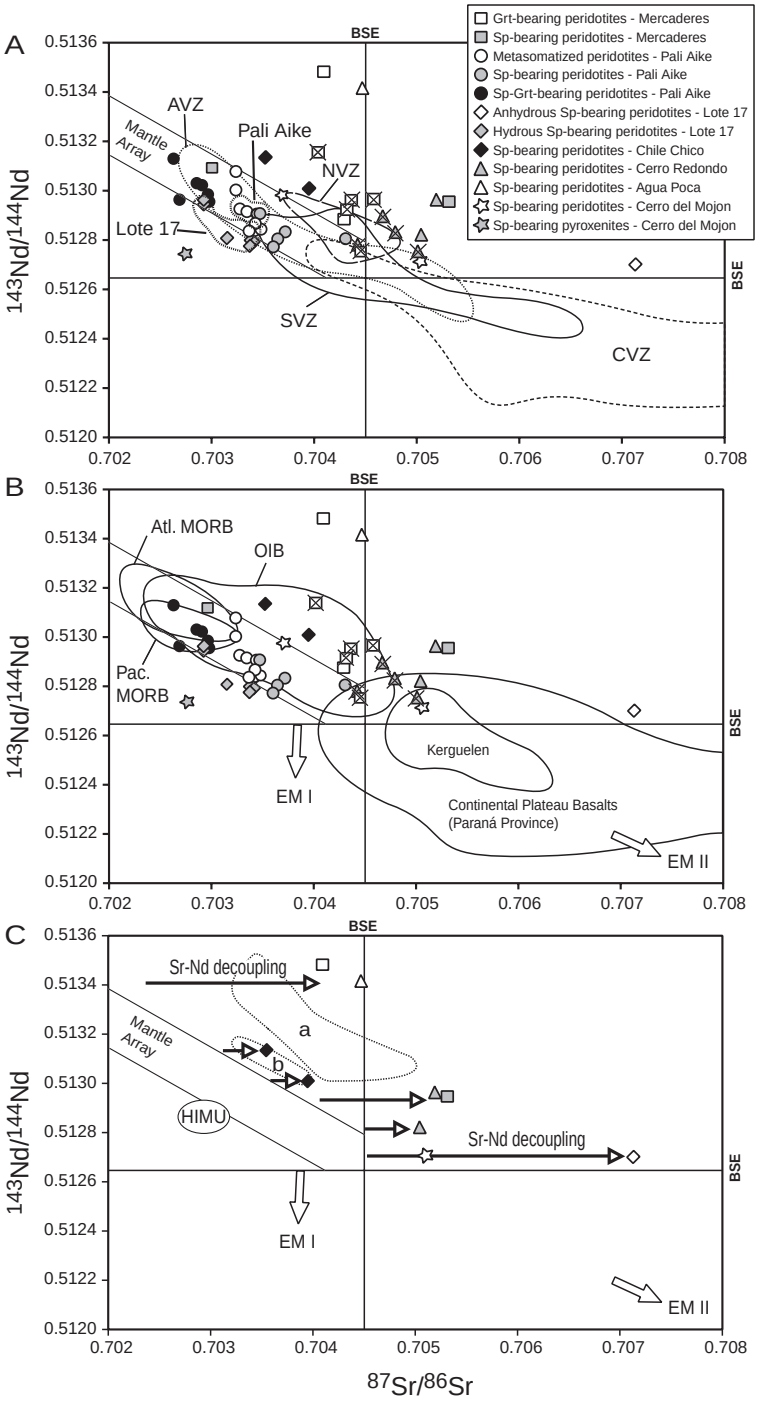

process, but still retaining characteristics of a fertile mantle, possibly caused by cryptic metasomatism by a fluid enriched in some incompatible elements. Neither trace nor REE pattern of this sample resemble any group of samples studied by Gorring and Kay (2000) from the same place, what express the complexity of melting and metasomatizing processes that the mantle from that area was exposed, producing a diversity of samples with different features.

Samples from Cerro Redondo show different degrees of HREE fractionation in relation to LREE enrichment (Fig. 3C), which is consistent with the different degree of host basalt contamination and metasomatism in the samples less contaminated by basalt (see also Schilling et al., 2005). Th, P and Hf positive anomalies together with Rb, K, Sm and Zr negative anomalies (Fig. 4C) characterize almost all the samples from this set, and can be explained by the metasomatic processes in the less contaminated samples by the host basalt.

5. Sr and Nd isotopes

The isotopic results are listed in Table 2 and displayed in Fig. 5. Consideration of the $^{87}Sr/^{86}Sr$ ratios indicates that Cerro del Mojon xenoliths have the most variable $^{87}Sr/^{86}Sr$ ratios, ranging from 0.71260 (which is the highest ratio among the studied samples, and very anomalous for a mantle xenolith) to 0.70269. $^{143}Nd/^{144}Nd$ ratios on these samples range from 0.51258, for the most Sr radiogenic enriched sample, to 0.51298. Lote 17 xenoliths have the second highest $^{87}Sr/^{86}Sr$ ratios, around 0.70650. Clinopyroxene from this sample has ratio of 0.70684 suggesting equilibrium with the whole rock. $^{143}Nd/^{144}Nd$ ratios for this rock and mineral separates are 0.51267 and 0.51263, respectively, suggesting that the isotopic equilibrium with respect to the Sm–Nd system was attained in this rock.

Cerro Redondo xenoliths present $^{87}Sr/^{86}Sr$ ratios from 0.70501 (($^{143}Nd/^{144}$/Nd=0.51276) to 0.70442 ($^{143}Nd/^{144}Nd$=0.51279). One sample, however is more enriched in radiogenic Sr, with $^{87}Sr/^{86}Sr$= 0.70519 ($^{143}Nd/^{144}Nd$=0.51297). Finally, comes the Mercaderes xenoliths with $^{87}Sr/^{86}Sr$ from 0.70534 to 0.70300 ($^{143}Nd/^{144}Nd$=0.51293 and 0.51316, respectively). Attempts to correlate the presence of garnet (and/or spinel) with isotopic data were unsuccessful. However, garnet peridotite seems to concentrate in a narrow $^{87}Sr/^{86}Sr$ range from 0.70389 to 0.70459 (Fig. 5), although they show the highest variation in $^{143}Nd/^{144}Nd$ ratios (from 0.51276 to 0.51348).

Plot of all Sr–Nd isotopic data on petrogenetic isotope diagram ($^{143}Nd/^{144}Nd$ vs. $^{87}Sr/^{86}Sr$) of Fig. 5A,B suggests that the majority of these samples are disposed in the mantle array, here defined as MORB–OIB–BSE trend (after De Paolo and Wasserburg, 1979). They are also in good agreement with the South America basaltic trend (Fig. 5A) defined by basalts from the four South American volcanic areas: NVZ, CVZ, SVZ and AVZ. However, some samples in this study plot outside these trends, showing an enrichment of radiogenic Sr without significant changes in the Nd isotopic ratios (Fig. 5C). Our following discussions will focuses on these anomalous samples.

6. Discussion

Melting, metasomatism, infiltration of host basalt and crustal alteration are processes usually used to explain chemical and mineralogical modifications of mantle xenoliths during and after their ascent from the mantle to the surface. As cited before in this work, some of the studied mantle xenolith samples present enrichment in radiogenic Sr without dramatic changes in the Nd isotopic system, which we call Sr–Nd decoupling. Such characteristic leads these samples to

Fig. 5. Sr–Nd isotopic composition (from this work and from literature for South American lithospheric mantle xenoliths. For comparison, the fields of mantle derived basalt from volcanic zones from South America (NVZ, CVZ, SVZ and AVZ—A) and MORB, OIB and continental basalts (B) are also plotted. Samples with basalt contamination (see text) have a "×" on the symbols. Tectonic setting fields were compiled from "http://georoc.mpch-mainz.gwdg.de/". OIB-field had drawn using Hawaii, La Palma, Azores, St. Helena, Easter and Ascension islands. In C, fields (a) and (b) correspond to Eastern China (Tatsumoto et al., 1992) and North Atlantic (Ionov et al., 2002) mantle xenoliths, respectively. Pali Aike field is from Stern et al. (1999), and Lote17 field (hydrous xenoliths) from Gorring and Kay (2000). EMI, EMII and HIMU correspond to enriched mantle I, enriched mantle II and to high U/Pb mantle composition, respectively defined by Tatsumoto et al. (1992). Arrows in C indicate the displacement to the right of the compositions of the studied mantelic samples.

plot outside the mantle array trend defined by De Paolo and Wasserburg (1979). The analytical procedures performed in our analyses (acid leaching of the samples previously to the acid digestion), together with the careful sample selection, minimize the crustal alteration effect, ruling out any crustal processes that could account for the radiogenic Sr increasing. Other processes are discussed below.

6.1. Contamination by the host basalt—how to evaluate sample affected by this process?

Evaluation of basalt contamination of the mantle xenoliths can done by petrographic textures, and plotting the host basalt and xenolith analyses in diagrams such as 1/Sr vs. $^{87}Sr/^{86}Sr$ and 1/Nd vs. $^{143}Nd/^{144}Nd$ (Fig. 6A–F). Linear trends in these

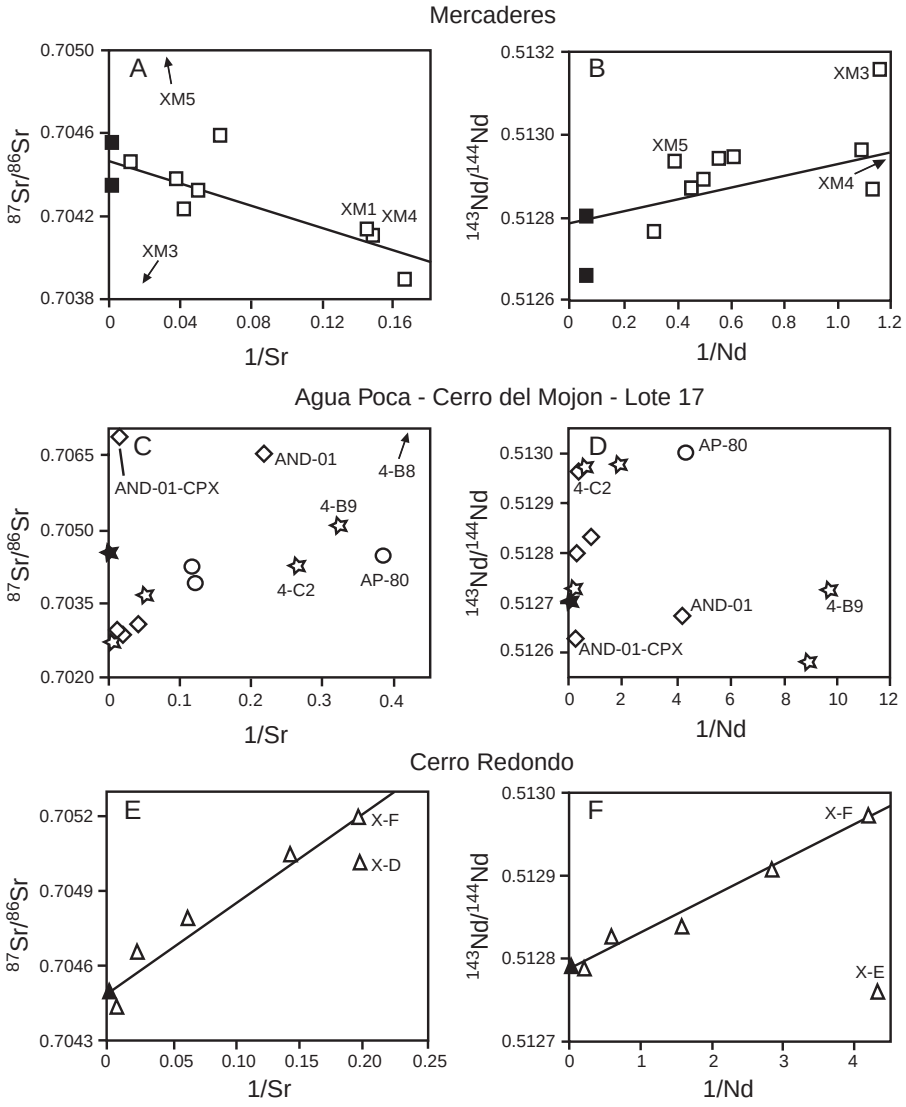

Fig. 6. Models of mixture through plots of 1/Sr vs. $^{87}Sr/^{86}Sr$ and 1/Nd vs. $^{143}Nd/^{144}Nd$. See text for details. Symbols as in Fig. 2. Labels next to symbols are sample names. Samples XM5 and XM3 (A), XM4 (B), AND-01-CPX and 4B8 (C) plot out of the scale of the figures and their positions are indicated by the arrows (see text). Sample AND-01-CPX corresponds to analyses performed in separated clinopyroxene from sample AND-01.

diagrams suggest that the samples situated in the middle of the trend could be explained by mixing processes of the samples situated in the extremity of the trend (Faure, 1986), usually represented by the host basalt (lower 1/Sr and 1/Nd ratios) and the less contaminated mantle xenolith sample (higher 1/Sr and 1/Nd ratios). Samples considered as less contaminated plot outside the trend, or as end member in the opposite side of the host basalt.

Most samples from the Mercaderes suite (Fig. 6A and B) show good correlation for both Sr and Nd systems, especially for garnet–peridotite in the Sr system. According to the criteria described above, the samples considered as less modified by the host basalt are XM-4, for the garnet–peridotite, and XM-1, XM-5 and XM-3, for spinel–pyroxenites. XM-4 and XM-1 are the end members in Fig. 6A. Although the Nd isotopic composition for XM-1 is not available, XM-4 is still the end member in Fig. 6B (the position is indicated by an arrow). Samples XM-5 and XM-3 plot out of the trend defined by all samples from Mercaderes in Fig. 6A (positions indicated by arrows) and in Fig. 6B.

The sample AP-80, from Agua Poca (Fig. 6C,D), is the less contaminated sample considering its high 1/Sr and 1/Nd values, compared to the other samples from the same suite.

Samples 4-C2, 4-B9 and 4-B8, from Cerro del Mojon (Fig. 6C,D), are the less contaminated considering their high 1/Sr and 1/Nd ratios. The presence of melt pockets associated with amphibole crystallization in sample 4-C2 suggests that metasomatic processes with melt percolation took place in this sample.

AND-01 is the only sample from Gobernador Gregores (Lote 17) region here isotopically analyzed for its whole rock and separated clinopyroxene. Both whole rock and clinopyroxene isotopic compositions of this sample plot in Fig. 6C,D far from the trend defined by the samples from the same region studied by Gorring and Kay (2000), shown in Fig. 6C,D. High 1/Nd and 1/Sr ratios suggest that this sample is not contaminated by the host basalt. This consideration is supported by lack of petrographic texture suggestive of host basalt contamination.

The samples X-D, X-E and X-F from Cerro Redondo (Fig. 6E,F) seem to be of less contaminated for similar reasons. Detailed descriptions and constraints on these samples can be found in Schilling et al. (2005).

6.2. Distribution of the samples in the Sr–Nd diagram

Distribution of the samples in Fig. 5A and B shows that radiogenic Nd decreases in the following sequence of xenolith suites: Mercaderes and Agua Poca>Cerro Redondo>Lote 17 and Cerro del Mojon.

All xenolith samples contaminated by the host basalts (samples in Fig. 5A and B with a "×" on the symbols) plot outside the trends defined by the mantle-derived magmas from the Andean volcanic zones (Fig. 5A) and by the MORB–OIB–BSE magmas (Fig. 5B—mantle array—De Paolo and Wasserburg, 1979). Samples not affected by the host basalt plot inside or outside these trends. Samples that plot outside of the MORB–OIB–BSE trend (Fig. 5B) are displaced to the right side of the mantle array, suggesting an enrichment of radiogenic Sr without significant changes in the Nd isotopic ratio. Such characteristic has also been observed in mantle xenolith samples from Eastern China (Tatsumoto et al., 1992), and in the North Atlantic region (Ionov et al., 2002), which are also displayed in Fig. 5C (a and b fields) for comparison. We consider that the component that introduced the anomalous radiogenic Sr to these xenoliths is likely of mantle origin (our laboratory procedures of leaching samples previously to the tri-acid digestion (see analytical procedures) would have eliminated any material resulted from superficial alteration product or supergenic carbonates). All samples that plot out of the MORB–OIB–BSE trend (the mantle array—Fig. 5B) have Sr/Nd ratios higher than that for the primitive mantle (around 18) of McDonough (1990). Exceptions are sample AP-80, which has lower ratio, and sample AND-01, which has a primitive ratio.

6.3. Constraints on the characteristics of the mantle modifying agent and processes using two-end-member mixing models

In order to better explore the mixing processes in the mantle as responsible for the Sr–Nd isotopic compositions of the xenolith samples studied here, we calculated the mixing line of mixtures between a depleted peridotite and an enriched source with

variable Sr/Nd ratio (Fig. 7) using the following equation (Faure, 1986):

$$R_M^x = \frac{R_A^x X_A f + R_B^x X_B (1-f)}{X_A f + X_B (1-f)}$$

where R_M^x is an isotope ratio of X in a mixture of components A and B, X_A and X_B are concentrations of X in A and B, and f is the weight fraction of A defined as:

$$f = \frac{A}{A+B}$$

where A and B are the weight of the two components in a given mixture.

The depleted mantle composition considered here was the same as the one chosen by Ionov et al. (2002), and corresponds to a residue of about 5% partial melting of a primitive spinel lherzolite (Sr/Nd PM ~15.5; Hoffmann, 1988; Sun and McDonough, 1989). However, the enriched end-member composition is an average of the Kerguelen OIB alkaline basalt samples from Storey et al. (1988), and Weis et al. (1993). This basalt is assumed to be derived directly from an uncontaminated mantle by melting processes. These samples were chosen due to their large range of Sr content (from 406 to 1044 ppm), without dramatically changing the Nd content (from 25 to 54 ppm). This condition gives these rocks Sr/Nd ratios ranging from 15 to 24. In our model, variable Sr compositions (from 588 to 5000 ppm) were chosen, but the $^{87}Sr/^{86}Sr$ and $^{143}Nd/^{144}Nd$ ratios and the Nd concentrations were kept constant. End-members' mixing lines, calculated for the depleted mantle and the enriched source with Sr compositions around 1500 and 2200 ppm (resulting in Sr/Nd around 44 and 65, respectively), are in good agreement with not contaminated xenolith samples, for the host basalt from Mercaderes, Agua Poca and Cerro Redondo localities, and some samples of the Cerro del Mojon locality (Fig. 7). The majority of the samples from Cerro del Mojon and sample AND-01 suggests a mixture of a depleted mantle and an enriched source with high $^{87}Sr/^{86}Sr$, low $^{143}Nd/^{144}Nd$ and high Sr content. This source has an EM-2 (enriched mantle II—Zindler and Hart, 1986) characteristic.

The problem to assume this modeling is the high Sr/Nd ratio attributed to the end member. Although high Sr/Nd ratios have been observed in mantle worldwide, they are not common in mantle-derived melts. Estimated primitive mantle Sr/Nd ratios, based on volcanic basaltic rocks (McDonough, 1990), vary around a mean value of 18, while depleted mantle

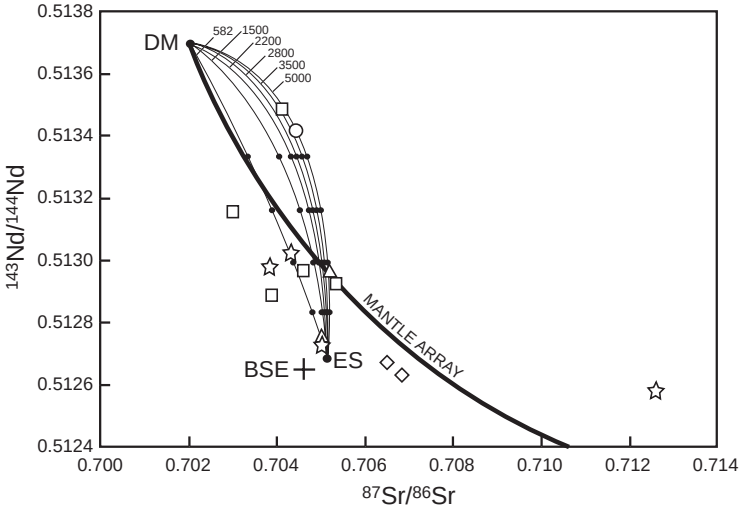

Fig. 7. Sr–Nd isotopic diagram of selected studied samples (see text). The mixing line (strong line, mantle array) represents a mixture of a depleted mantle (DM=MORB) and an enriched source (continental basalt, which plots outside of the diagram). The mixing lines shown are calculated for the mixture of a depleted mantle (DM=MORB) and an enriched source (ES) with variable Sr/Nd ratios (see text). BSE (bulk earth silicate) position (cross symbol) is shown for reference. Symbols as in Fig. 2.

ratios are lower (around 13). Carbonatite melts, however, show large variation of this ratio (from primitive mantle values around 18 to 122), which makes these melts the best metasomatic agent end member. Xenoliths from South America with well-known infiltration of carbonatitic melts (Stern et al., 1999, Gorring and Kay, 2000) are represented in Fig. 5A and B by the xenoliths from Lote 17 and from Pali Aike peridotites. Lote 17 samples, despite the carbonatite influence, generally plot to the left side of the MORB–OIB–BSE trend, while just one sample from Pali Aike plots to the right side. Such evidence does not support the hypothesis that carbonatite melts could be the metasomatic agent end member. High Sr/Nd ratios are also observed in pelagic sediments (around 50; PETDB—petrological data base of the ocean floor—http://petdb.ldeo.columbia.edu/petdb/) and in arc-volcanic basalts (up to 40; McCulloch and Gamble, 1991). In the first case, there is enrichment in the $^{87}Sr/^{86}Sr$ ratios up to 0.720 and the model does not apply (Fig. 7). However, arc-volcanic basalts, probably originated by a mixture of mantle-derived and slab-derived melts (McCulloch and Gamble, 1991; White and Patchett, 1984), have high Sr/Nd ratios (40 to 45; McCulloch and Gamble, 1991; White and Patchett, 1984) but low $^{87}Sr/^{86}Sr$ ratios (around 0.704 to 0.705), and could be considered as the end member that could metasomatise the mantle that originated the xenolith samples studied here. Modeling of mixture between depleted mantle and arc-basalt from the Antilles (White and Patchett, 1984) in which Sr/Nd ratio is around 33.8, show good agreements with all samples studied here.

6.4. Alternative process to explain the Sr–Nd decoupling

Based on the trace element composition and isotopic data, we conclude that two-component-mixing modeling, in which one of the end members is the depleted mantle and the other is an arc-basalt-derived melt, would explain the enriched radiogenic contents of the samples that plot on the right side of the mantle array. However, any process that could enrich preferentially the contents of Sr without simultaneous enrichment in Nd could explain the position of these samples in Figs. 5A,B,C and 7. Some authors have been arguing that a chemical fractionation, in which Sr contents increases faster than Nd content, could happen when a melt percolates a peridotite matrix due to a chromatographic effect. The chromatographic effect is controlled by the duration of the liquid (metasomatic agent) percolation through the solid matrix (mantle), and by physical and chemical properties such as matrix porosity, melt viscosity and density, matrix–melt element partition and diffusion coefficients.

A simplistic equation (Navon and Stolper, 1987) that could explain such effect is:

$$\frac{\partial C_{f,i}}{\partial t} + \frac{\phi\rho_f}{\phi\rho_f + (1-\phi)\rho_s K_d} V_f \frac{\partial C_{f,i}}{\partial z} = 0$$

where: ϕ is the fluid (metasomatic agent) fraction; ρ_f and ρ_s are the fluid and solid matrix (mantle) densities, respectively; $C_{f,i}$ and $C_{s,i}$ are the concentration of the element i (in weight %) in the fluid and solid matrix, respectively; K_d is the element distribution coefficient; and V_f is the fluid velocity during percolation in the solid matrix.

Some authors suggest that the chromatographic effect would have several influences on isotopic data (Navon and Stolper, 1987; Reiners, 1998; Bodinier et al., 1990; Vasseur et al., 1991; De Paolo, 1996; Bedini et al., 1997; Hauri, 1997). As melt percolates into the peridotite matrix, trace element composition of the melt closer to the percolation front becomes increasingly equilibrated with the host peridotite. However, as new input of melt happens, the abundance of elements in the advancing melt changes at different rates. As peridotite trace element composition is basically controlled by the partition coefficient in clinopyroxenes ($D^{cpx/melt}$), elements with higher $D^{cpx/melt}$ (Nd, for instance) are selectively removed from the liquid into the peridotite during the melt migration, at the same time that elements with lower $D^{cpx/melt}$ (Sr, for instance) will be enriched in the melt. Then Sr will travel faster than Nd in the melt. Such effect will increase the Sr/Nd ratio in the liquid, but will decrease this ration in the matrix. If we calculate the mixing lines between these two end members (a depleted mantle matrix that suffered the percolation of a enriched melt and in which the chromatographic effect took place) considering the chromato-

graphic effect to the corrected point where this melt-enrichment coeval to the matrix-depletion, the curve will mimic those plotted in Fig. 7. As a result, there will be increasing radiogenic Sr isotopic ratios without dramatic modification of Nd radiogenic ratios.

7. Conclusions

Most of the Andean subduction-related mantle xenoliths studied here and from literature plots along the "normal" MORB–OIB–BSE trend (mantle array; De Paolo and Wasserburg, 1979). However, in some mantle xenoliths from the Northern, Southern and Austral Andean volcanic zones, we observed anomalous Sr–Nd isotopic compositions, which make these samples plotting outside the "mantle array" trend. These anomalous results reflect distinctly processes that took place in the mantle and are related to: i) mixture of a depleted mantle with an enriched source (EM-2), as observed here for two samples (one from Lote 17 and another from Cerro del Mojon) due to higher $^{87}Sr/^{86}Sr$ and lower $^{143}Nd/^{144}Nd$ ratios; ii) mixture of a depleted mantle with a mixture of mantle-derived and slab-derived melts. This latter had high Sr/Nd ratios but low $^{87}Sr/^{86}Sr$ ratios, as observed for some samples of Mercaderes and Agua Poca xenolith suites; and iii) chromatographic processes, as observed in these samples, one from Agua Poca and another from Mercaderes, which exhibit enrichment of radiogenic Sr without dramatic change of Nd isotopic composition. Processes that took place after/during the transport of the mantle fragment to the surface, as crustal weathering and host basalt contamination could change the $^{87}Sr/^{86}Sr$ and $^{143}Nd/^{144}Nd$ ratios of the samples, but could not explain the disposal of the mantle-derived samples to the right side of the mantle array in Fig. 5A,B,C.

Acknowledgments

Our special thanks to F. Chemale, Jr., Koji Kawashita, C.A. Cingolani and F. Hervé for valuable help. This research was supported by funding from CNPq-PROSUL (project AC-74) and we are grateful to the facilities available at Laboratório de Geologia Isotópica of Universidade Federal do Rio Grande do Sul. We also thank the important comments and suggestions of the anonymous reviewers and guest editors.

References

Bedini, R.M., Bodinier, J.L., Dautria, J.M., Morten, L., 1997. Evolution of LILE-enriched small melt fractions in the lithospheric mantle: a case study from the East African Rift. Earth Planet. Sci. Lett. 153, 67–83.

Bertotto, G.W., 2000. Cerro Agua Poca, un cono basaltico cuaternario portador de xenolitos ultramaficos, en el oeste de la provincia de La Pampa, Argentina. Rev. Asoc. Geol. Argent. 55 (1–2), 59–71.

Bertotto, G.W., 2003. Evolución geológica y petrológica de los conos basálticos Cenozóicos portadores de xenólitos ultramáficos del Margen Oriental de la província basáltica Andino Cuyana, Provincias de La Pampa y Mendoza. PhD thesis, Universidad Nacional de La Plata, 179p.

Bodinier, J.L., Vasseur, G., Vernières, J., Dupuy, C., Fabriès, J., 1990. Mechanisms of mantle metasomatism: geochemical evidence for the Lhez orogenic peridotite. J. Pet. 31, 597–628.

Brey, G.P., Köhler, T., 1990. Geothermobarometry in four-phase lherzolites: II. New thermobarometers, and practical assessment of existing thermobarometers. J. Petrol. 31, 1353–1378.

Conceição, R.V., Green, D.H., 2000. Behavior of the cotectic curve Em-Ol in the system leucite–olivine–quartz under dry conditions to 2.0 GPa. Geochem. Geophys. Geosyst. 1, 122–123 (paper No. 200GC000071).

Conceição, R.V., Green, D.H., 2004. Derivation of potassic (shoshonitic) magmas by decompression melting of phlogopite+pargasite lherzolite. Lithos 72, 209–229.

Conceição, R.V., Koester, E., Mallmann, G., Kawashita, K., Chemale Jr., F., Cingolani, C., Hervé, F., Bertotto, G.W., Schilling, M., Rodriguez-Vargas, A., Weber, M.B.I., Morata, D., Espinoza, F., 2003. New insights on the Andean-related subcontinental lithospheric mantle and evidence of Sr–Nd decoupling. IV South American Symposium on Isotope Geology, Salvador, Brazil, Extended Abstracts, pp. 528–531.

De Paolo, D.J., 1996. High-frequency isotopic variations in the Mauna Kea tholeiitic basalt sequence: melt zone dispersivity and chromatography. J. Geophys. Res. 101, 11855–11864.

De Paolo, D.J., Wasserburg, G.J., 1979. Petrogenetic mixing models and Nd–Sr isotopic patterns. Geochim. Cosmochim. Acta 43, 615–627.

Faure, G., 1986. Principles of Isotopic Geology. John Wiley and Sons, Inc., New York. 589 pp.

Godard, M., Bodinier, J.L., Vasseur, G., 1995. Effects of mineralogical on trace element redistributions in mantle rocks during percolation processes—a chromatographic approach. Earth Planet. Sci. Lett. 3 (3–4), 444–461.

Gorring, M.L., Kay, S.M., 2000. Carbonatite metasomatized peridotite xenoliths from southern Patagonia: implications for lithospheric process and Neogene plateau magmatism. Contrib. Mineral. Petrol. 140, 55–72.

Hauri, E.H., 1997. Melt migration and mantle chromatography: 1. Simplified theory and conditions for chemical and isotopic decoupling. Earth Planet. Sci. Lett. 153, 1–19.

Hirschman, M.M., Baker, M.B., Stolper, E.M., 1998a. The effect of alkalis on the silica content of mantle derived magmas. Geochim. Cosmochim. Acta 62, 883–902.

Hirschmann, M.M., Ghiorso, M.S., Waslenki, L.E., Asimow, P.D., Stolper, E.M., 1998b. Calculation of peridotite partial melting from thermodynamic models of minerals and melts: I. Review of methods and comparison with experiments. J. Petrol. 39, 1091–1115.

Hoffmann, A.W., 1988. Chemical differentiation of the Earth: the relationship between mantle, continental crust, and oceanic crust. Earth Planet. Sci. Lett. 90, 297–314.

Ionov, D.A., Mukasa, S.B., Bodinier, J.-L., 2002. Sr–Nd–Pb isotopic composition of peridotite xenoliths from Spitsbergen: numerical modeling indicates Sr–Nd decoupling in the mantle by melt percolation metasomatism. J. Petrol. 43, 2261–2278.

Köhler, T.P., Brey, G.P., 1990. Calcium exchange between olivine and clinopyroxene calibrated as a geothermobarometer for natural peridotites from 2 to 60 kb with applications. Geochim. Cosmochim. Acta 54, 2357–2388.

McCulloch, M.T., Gamble, J.A., 1991. Geochemical and geodynamical constraints on subduction zone magmatism. Earth Planet. Sci. Lett. 102, 358–374.

McDonough, W.F., 1990. Constraints on the composition of the continental lithospheric mantle. Earth Planet. Sci. Lett. 101, 1–18.

McDonough, W.F., Frey, F.A., 1989. Rare earth elements in upper mantle rocks. In: Lipin, B.R., McKay, G.A. (Eds.), Geochemistry and Mineralogy of Rare Earth Elements. Mineralogical Society of America, Washington, DC, pp. 99–145.

McKenzie, D.P., 1984. The generation and compaction of partially molten rock. J. Petrol. 25, 713–765.

Menzies, M.A., Hawkesworth, C.J., 1987. Mantle Metasomatism. Academic Press, London. 422 pp.

Mercier, J.C., Nicolas, A., 1975. Textures and fabrics of upper-mantle peridotites as illustrated by xenoliths from basalts. J. Petrol. 16, 454–487.

Mercier, J.C., Benoit, V., Girardeau, J., 1984. Equilibrium state of diopside-bearing harzburgites from ophiolites: geobarometric and geodynamic implications. Contrib. Mineral. Petrol. 85, 391–403.

Mukasa, S.B., Wilshire, H.G., 1997. Isotopic and trace element compositions of upper mantle and lower crustal xenoliths, Cima volcanic field, California; implications for evolution of the sub-continental lithospheric mantle. J. Geophys. Res. 102, 20133–20148.

Navon, O., Stolper, E., 1987. Geochemical consequences of melt percolation: the upper mantle as a chromatographic column. J. Geol. 95, 285–307.

Ramos, V.A., 1999. Plate tectonic setting of the Andean Cordillera. Episodes 22, 183–190.

Reiners, P.W., 1998. Reactive melt transport in the mantle and geochemical signatures of mantle-derived magmas. J. Petrol. 39, 1039–1061.

Ringwood, A.E., 1982. Phase transformations and differentiation in subducted lithosphere: implications for the mantle dynamics, basalt petrogenesis, and crustal evolution. J. Geol. 90, 611–643.

Rodriguez-Vargas, A., Koester, E., Mallmann, G., Conceição, R.V., Kawashita, K., Weber, M.B.I., 2005. Mantle diversity beneath the Colombian Andes, Northern Volcanic Zone: constraints on Sr and Nd isotopes. Lithos 82, 471–484 (this volume).

Schilling, M., Conceição, R.V., Mallmann, G., Koester, E., Kawashita, K., Hervé, F., Morata, D., Motoki, A., 2005. Spinel mantle xenoliths from Cerro Redondo, Argentine Patagonia: petrographic, geochemical and isotopic evidence of interaction between xenoliths and host basalt. Lithos 82, 485–502 (this volume).

Stern, C.R., Killian, R., Olker, B., Hauri, E.H., Kyser, T.K., 1999. Evidence from mantle evolution for relatively thin (<100 km) continental lithosphere below the Phanerozoic crust of southernmost South America. Lithos 48, 217–235.

Storey, M., Saunders, A.D., Tarney, J., Leat, P., Thirlwall, M.F., Thompson, R.N., Menzies, M.A., Marriner, G.F., 1988. Geochemical evidence for plume–mantle interactions beneath Kerguelen and Heard Islands, Indian Ocean. Nature 336, 371–374.

Sun, S.S., McDonough, W.F., 1989. Chemical and isotopic systematics of oceanic basalts: implications for mantle composition and processes. In: Sounders, A.D., Norry, M.J. (Eds.), Magmatism in the Ocean Basins. Geological Society London Special Publication vol. 42, pp. 313–345.

Tatsumoto, M., Basu, A.R., Wankang, H., Junwen, W., Guanghong, X., 1992. Sr, Nd and Pb isotopic of ultramafic xenoliths in volcanic rocks of Eastern China: enriched components EMI and EMII in subcontinental lithosphere. Earth Planet. Sci. Lett. 113, 107–128.

Thompson, R.N., 1982. Magmatism of the British tertiary volcanic province. Scott. J. Geol. 18, 49–107.

Vasseur, G., Vernières, J., Bodinier, J.L., 1991. Modeling of trace element transfer between mantle melt and heterogranular peridotite matrix. J. Petrol. Spec. Vol., 41–54.

Weber, M.B.I., 1998. The Mercaderes–Rio Mayo xenoliths, Colombia: their bearing on mantle and crustal processes in the Northern Andes. PhD thesis, University of Leicester, UK, 277 p.

Weis, D., Frey, F.A., Leyrit, H., Gautier, I., 1993. Kerguelen Archipelago revisited: geochemical and isotopic study of the SE Province lavas. Earth Planet. Sci. Lett. 118, 101–119.

White, W.M., Patchett, P.J., 1984. Hf–Nd–Sr isotopes and incompatible element abundances in island arcs: implications for magma origins and crust–mantle evolution. Earth Planet. Sci. Lett. 67, 167–185.

Wood, B.J., Banno, S., 1973. Garnet–orthopyroxene and orthopyroxene–clinopyroxene relationships in simple and complex systems. Contrib. Mineral. Petrol. 42, 109–124.

Yaxley, G.M., Crawford, A.J., Green, D.H., 1991. Evidence for carbonatite metasomatism in spinel peridotite xenoliths from western Victoria, Australia. Earth Planet. Sci. Lett. 107, 305–317.

Yaxley, G.M., Green, D.H., Kamenetsky, V., 1998. Carbonate metasomatism in the southeastern Australian lithosphere. J. Petrol. 39, 1917–1931.

Zindler, A., Hart, S.A., 1986. Chemical geodynamics. Annu. Rev. Earth Planet. Sci. 14, 493–571.